Slow photoelectron velocity-map imaging spectroscopy of C_2N^-, C_4N^-, and C_6N^-

Etienne Garand,[1] Tara I. Yacovitch,[1] and Daniel M. Neumark[1,2,a)]
[1]*Department of Chemistry, University of California, Berkeley, California 94720, USA*
[2]*Chemical Sciences Division, Lawrence Berkeley National Laboratory, Berkeley, California 94720, USA*

(Received 21 November 2008; accepted 8 January 2009; published online 11 February 2009)

High resolution photoelectron spectra of C_2N^-, C_4N^-, and C_6N^- anions are reported, obtained using slow electron velocity-map imaging. The spectra show well resolved transitions to the $\tilde{X}\ ^2\Pi$ neutral ground state of all three species and to the $\tilde{a}\ ^4\Sigma^-$ excited state of C_2N and C_4N. This study yields the adiabatic electron affinity of C_2N, C_4N, and C_6N, the spin-orbit splitting in the $\tilde{X}\ ^2\Pi$ state of each radical, and the term energy of the $\tilde{a}\ ^4\Sigma^-$ state in C_2N and C_4N. Relatively little vibrational activity is observed, indicating small geometry changes upon photodetachment. This result, plus the observation of transitions to neutral quartet states, indicates that the $C_{2n}N^-$ $(n=1-3)$ anions all have linear $^3\Sigma^-$ ground states. © *2009 American Institute of Physics*. [DOI: 10.1063/1.3076320]

I. INTRODUCTION

The nitrogen-doped carbon chains (C_nN) are important interstellar constituents. The three smallest members of the series with odd numbers of carbon atoms, CN, C_3N, and C_5N, have been detected[1–4] in the interstellar medium. Recently, the C_3N^- anion has also been detected[5] in the circumstellar envelope of the evolved carbon star IRC+10216. In contrast, none of the members of the $C_{2n}N$ series have yet been detected in interstellar sources even though these species are predicted to play a role in the interstellar chemistry.[6,7] Their detection by means of radio astronomy is greatly hindered by their small dipole moments.[8] With the exception of C_2N, experimental information on the $C_{2n}N$ species is relatively sparse. In this paper, high-resolution photoelectron spectra of the C_2N^-, C_4N^-, and C_6N^- anions are reported that provide a detailed probe of these anions and the corresponding neutral species.

The C_2N radical has been the subject of numerous experimental and theoretical studies since its first identification by Merer and Travis[9] in 1965, many of which have focused on the strong Renner–Teller (RT) interaction in its $\tilde{X}\ ^2\Pi$ ground state. C_2N has been investigated by UV and IR absorptions,[9–15] laser-induced fluorescence,[16–19] Fourier-transform emission spectroscopy,[20] microwave spectroscopy,[21] and laser magnetic resonance spectroscopy.[22] Gabriel *et al.*[23] calculated the RT perturbed rovibronic levels in its $\tilde{X}\ ^2\Pi$ state using variational methods. Excited state molecular orbital configurations, geometries, and vibrational frequencies were computed by Pd and Chandra[24] at the complete active space SCF (CASSCF) level. The C_4N and C_6N radicals have been studied experimentally by microwave spectroscopy[25] and theoretically using density functional theory (DFT).[26–28]

The only experimental information on $C_{2n}N^-$ anions comes from mass spectrometry studies in which the anions were produced by laser ablation[29,30] or sputtering.[31] Both experiments yielded strong even-odd alternations with the $C_{2n}N^-$ ions being considerably less intense than the $C_{2n+1}N^-$ ions. Second-order Møller–Plesset (MP2) calculations by Zhan and Iwata[32] found singlet ground states for $C_{2n}N^-$ $(n=1-3)$ with C_4N^- and C_6N^- having strongly bent geometries. However, a subsequent DFT study by Pascoli and Lavendy[33] yielded linear triplet ground states and low-lying singlet excited states for these same anions.

In this paper, we report photoelectron (PE) spectra of C_2N^-, C_4N^-, and C_6N^- anions obtained with slow electron velocity-map imaging (SEVI). The high resolution afforded by SEVI shows well resolved transitions to the $\tilde{X}\ ^2\Pi$ neutral ground state of all three species and to the $\tilde{a}\ ^4\Sigma^-$ excited state of C_2N and C_4N. These transitions are assigned with the help of electronic structure calculations. We obtain accurate electron affinities for all three radicals and term energies for the $\tilde{a}\ ^4\Sigma^-$ states in C_2N and C_4N. The observation of relatively little vibrational activity and transitions to neutral quartet states indicates that the $C_{2n}N^-$ $(n=1-3)$ anions have linear $^3\Sigma^-$ ground states.

II. EXPERIMENTAL

The SEVI apparatus has been described in detail elsewhere,[34–36] although a new ion source configuration was used in these studies. SEVI is a high resolution variant of PE spectroscopy in which mass-selected anions are photodetached at a series of wavelengths. The resulting photoelectrons are collected by velocity-map imaging[37] (VMI) using relatively low extraction voltages, with the goal of selectively detecting slow electrons with high efficiency and enlarging their image on the detector. At each wavelength, one obtains a high resolution photoelectron spectrum over a limited range of electron kinetic energy.

C_2N^- anions were produced from of a gas mixture comprising 0.005% acetonitrile (CH_3CN) in argon while C_4N^-

a)Author to whom correspondence should be addressed. Electronic mail: dneumark@berkeley.edu.

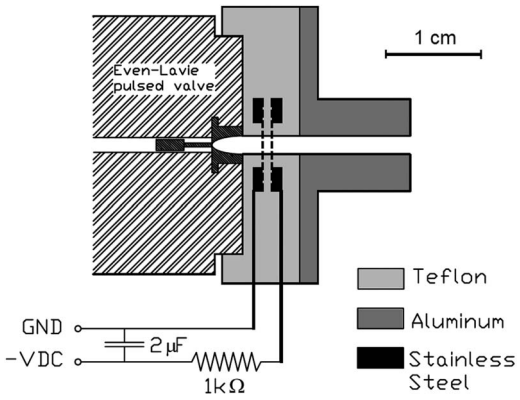

FIG. 1. Diagram of the grid discharge source.

and C_6N^- anions were produced from a mixture of 0.05% acetylene and 2% N_2O in a balance of argon. The gas mixture, at a stagnation pressure of 300 psi, was expanded into the source vacuum chamber through an Even–Lavie pulsed valve.[38] Anions were formed using the grid discharge source shown in Fig. 1. Here, the gas from the pulsed valve passed through a 2.5 mm×23 mm canal made from Teflon and aluminum, within which were two fine grids made of stainless steel wire mesh that were separated by 1 mm. The first grid was held to ground while the second was floated to around −500 V_{dc} through a 1 kΩ resistor. The passage of the expanding gas through the grids induced a discharge which produced the anions. In contrast to the pulsed discharge design of Osborn *et al.*,[39] this source does not require a high-voltage pulse or an external source of electrons for continuous stable operation. More importantly, the grid discharge source produces internally colder anions than the ionization source used previously on this instrument.[35,40,41] This attribute is crucial for SEVI in which the width of the unresolved rotational envelope of each peak limits the achievable resolution.

Anions produced by the source were perpendicularly extracted into a Wiley–McLaren time-of-flight mass spectrometer[42] and directed to the detachment region by a series of electrostatic lenses and pinholes. A pulse on the last ion deflector allowed only the desired mass into the interaction region. Anions were photodetached between the repeller and the extraction plates of the VMI stack by the gently focused output of a Nd:yttrium aluminum garnet pumped tunable dye laser. The photoelectron cloud formed was coaxially extracted down a 50 cm flight tube and mapped onto a detector comprising a chevron-mounted pair of time-gated, imaging quality microchannel plates coupled to a phosphor screen, as is typically used in photofragment imaging experiments.[43] Events on the screen were collected by a 1024×1024 charge-coupled device camera and sent to a computer. Electron velocity-mapped images resulting from 30 000 to 100 000 laser pulses were summed, quadrant symmetrized, and inverse-Abel transformed.[44] Photoelectron spectra were obtained via angular integration of the transformed images.

The apparatus was calibrated by acquiring SEVI images of atomic S^- and $C1^-$ at several different photon energies. With the 350 V VMI repeller voltage used in this study, the full widths at half maximum of the chloride peaks were 3.3 at 24 cm^{-1} above threshold. In the SEVI experiment, within the same image, all observed transitions have similar pixel widths (Δr), which means transitions observed further from threshold (larger r) are broader in energy. By varying the laser wavelength, a series of images in which the transitions of interest are close to a particular detachment threshold can be acquired, yielding a complete, high resolution photoelectron spectrum. The spectra presented here are plotted with respect to electron binding energy (eBE), defined as the difference between the photodetachment photon energy and the measured electron kinetic energy.

SEVI also provides information on the photoelectron angular distribution (PAD). For one-photon detachment, the PAD is given by[45,46]

$$\frac{d\sigma}{d\Omega} = \frac{\sigma_{\text{total}}}{4\pi}\left(1 + \beta\left(\frac{3}{2}\cos^2(\theta) - \frac{1}{2}\right)\right), \quad (1)$$

where θ is the angle between the direction of the photoelectron ejection and the polarization vector of the incident photon. The anisotropy parameter β lies between 2 and −1. It provides information on the orbital angular momentum (l) of the ejected photoelectron and hence the symmetry of the molecular orbital from which detachment occurs; $l=0$ (s-wave) detachment leads to $\beta=0$, $l=1$ (p-wave) to $\beta=2$, and $l=0$ and 2 in equal amplitude ($s+d$ wave) to $\beta=-1$. Generally, the value of β depends on the detachment energy[47] and thus peaks having $\beta>0$ are simply labeled as p while those with $\beta<0$ are labeled as $s+d$.

III. EXPERIMENTAL RESULTS

SEVI spectra of C_2N^-, C_4N^-, and C_6N^- are presented in Figs. 2–4. The peak positions, PADs, and assignments (see Sec. V) are summarized in Tables I–III. The spectra all display very similar features and are divided into two bands of peaks, separated by about 1 eV, with different PADs. The maximum eBE for each trace corresponds to the photon energy used in collecting the spectrum. Spectra taken at higher photon energy [upper traces in Figs. 3(a)] probe a wider energy window but yield poorer resolution for the features at lower eBE (i.e., faster electrons).

The traces in Figs. 2(a) and 3(a) are dominated by two peaks, A and B, with spacings varying from 29 to 38 cm^{-1}. All three spectra show two or three small peaks (a, b, and c) at slightly lower eBE than peaks A and B. The C_2N^- spectrum shows a smaller peak C lying at 456 cm^{-1} higher eBE than peaks A and B, while the C_4N^- and C_6N^- spectra show two smaller peaks, C and D, at higher eBE. All peaks in these three panels have $s+d$ PADs.

Figures 2(b) and 3(b) show transitions to a higher energy band comprising a large peak E and a much smaller peak F. The spacings between peaks A and E are 8413 cm^{-1} for C_2N^- and 9256 cm^{-1} for C_4N^-. All features in Figs. 2(b) and 3(b) have p PADs, suggesting that they arise from photodetachment from a different molecular orbital than the peaks in Figs. 2(a) and 3(a).

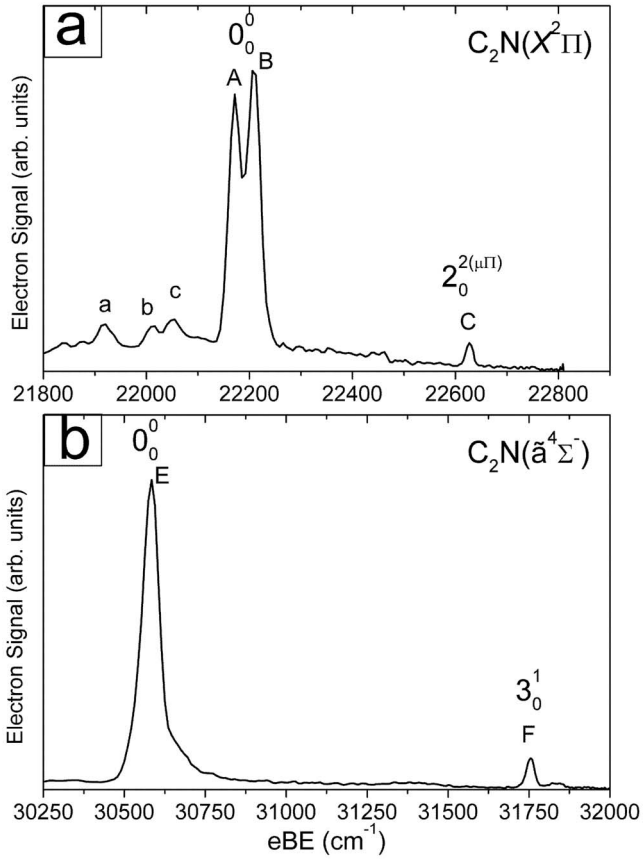

FIG. 2. SEVI spectra of C_2N^- covering the electron binding energy ranges of 21 800–22 900 cm^{-1} (panel a) and 30 250–32 000 cm^{-1} (panel b).

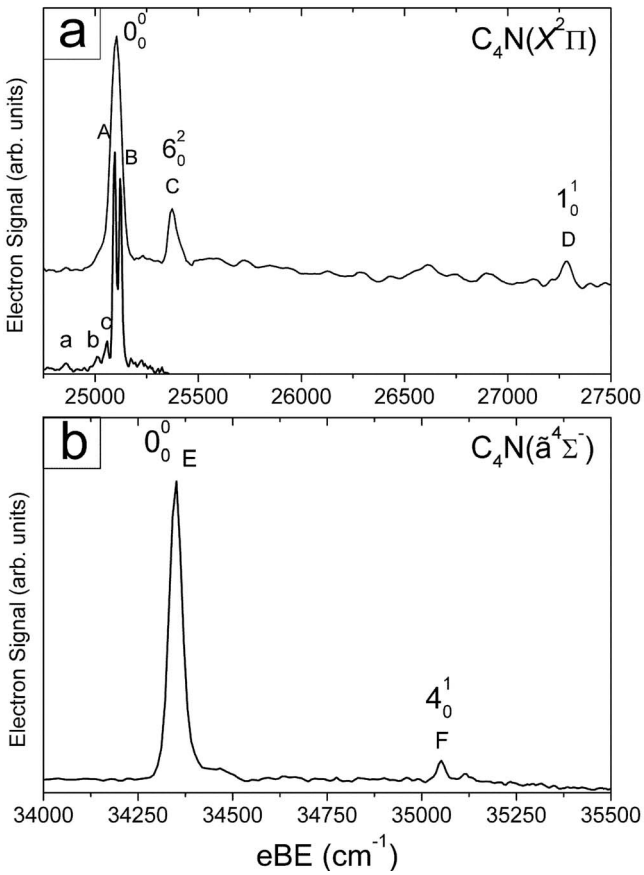

FIG. 3. SEVI spectra of C_4N^- covering the electron binding energy ranges of 24 750–26 000 cm^{-1} (panel a) and 34 000–35 500 cm^{-1} (panel b).

IV. ELECTRONIC STRUCTURE CALCULATIONS

Electronic structure calculations were performed on the relevant neutral and anionic states of $C_{2n}N$, as determined by previous studies.[24,26–28,30,32,33,48] The current calculations serve to produce, at a uniform level of theory, all the geometries and vibrational frequencies necessary to interpret the photoelectron spectra. Our calculations were carried out with DFT using the Becke three-parameter Lee, Yang, and Parr exchange-correlation functional[49,50] (B3LYP) and the augmented correlation consistent polarized valence triple-zeta basis set[51] (aug-cc-pVTZ). All computations were performed using the GAUSSIAN03 program.[52]

The calculated geometries of the anion $^3\Sigma^-$ state as well as the neutral $\tilde{X}\,^2\Pi$ and $\tilde{a}\,^4\Sigma^-$ states are shown in Fig. 5, while the harmonic vibrational frequencies and relative energies of the different species are presented in Table IV. The calculated anion geometries are essentially identical to those reported by Pascoli and Lavendy[33] using the same functional and basis set. The bent singlet states of the anion are not considered here. For the two neutral states of C_2N considered here, the DFT calculations yield shorter CC bond lengths than the CASSCF calculations of Pd and Chandra.[24] The C_4N and C_6N ground state bond lengths and frequencies calculated here are similar to previous DFT studies using smaller basis sets.[26–28] All the C_4N and C_6N bending modes in the $\tilde{X}\,^2\Pi$ state are nondegenerate in the calculations, as expected for vibrational modes subject to RT coupling. Calculated geometries, harmonic frequencies and energetics of the $\tilde{a}\,^4\Sigma^-$ state of C_4N and C_6N are reported for the first time.

Figure 5 emphasizes the geometry changes that occur upon photodetachment. All three species show a lengthening of the C_1–C_2 bond and a contraction of the neighboring bond upon photodetachment to the $\tilde{X}\,^2\Pi$ state. In C_4N, the four carbon atoms are approximately equally spaced in the anion, with a much more noticeable bond alternation in the

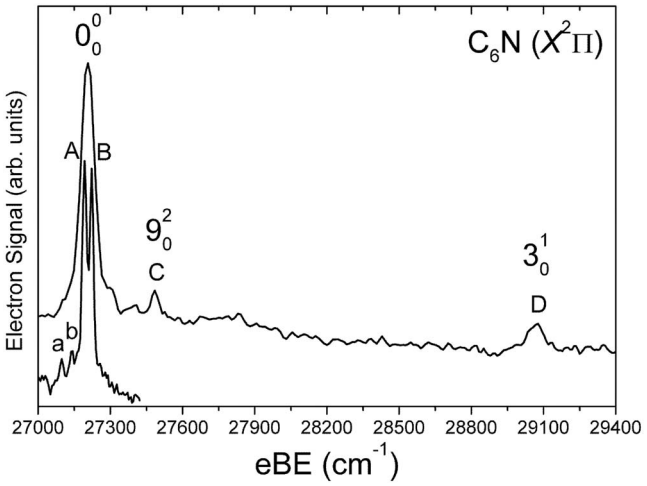

FIG. 4. SEVI spectra of C_6N^- covering the electron binding energy range of 27 000–29 400 cm^{-1}.

TABLE I. Peak positions, angular distributions, and assignments for the C_2N^- SEVI spectra.

Peak	Position (cm^{-1})	Offset (cm^{-1})	PAD	Assignments	
				Vibs	Electronic states
a	21 920	−232		$2_1^{1(\mu\Sigma)}$	$X\,^2\Pi \leftarrow X\,^3\Sigma^-$
b	22 015	−137		$2_1^{1(\Delta_{5/2})}$	$X\,^2\Pi \leftarrow X\,^3\Sigma^-$
c	21 852	−100		$2_1^{1(\Delta_{3/2})}$	$X\,^2\Pi \leftarrow X\,^3\Sigma^-$
A	22 171	0	*s*+*d*	0_0^0	$X\,^2\Pi_{1/2} \leftarrow X\,^3\Sigma^-$
B	22 209	38	*s*+*d*	0_0^0	$X\,^2\Pi_{3/2} \leftarrow X\,^3\Sigma^-$
C	22 627	456	*s*+*d*	$2_0^{2(\mu\Pi_r)}$	$X\,^2\Pi \leftarrow X\,^3\Sigma^-$
E	30 584	8413	*p*	0_0^0	$\tilde{a}\,^4\Sigma^- \leftarrow X\,^3\Sigma^-$
F	31 754	9583	*p*	3_0^1	$\tilde{a}\,^4\Sigma^- \leftarrow X\,^3\Sigma^-$

neutral characteristic of acetylenic (C–C≡C–C) bonding. In C_6N, the carbon atoms C_1-C_4 show alternating bond lengths in the anion and neutral, but the phase of the alternation flips upon photodetachment. In all three species, the C–N bond contracts upon detachment to the ground state, but the extent of this contraction decreases with increasing chain length.

V. ANALYSIS AND DISCUSSION

In this section, a detailed assignment of the SEVI spectra is presented, starting with the electronic bands in the upper and lower panels of Figs. 2 and 3. The splittings between peaks *A* and *E* in those spectra are similar to the calculated splittings in Table IV between the neutral $\tilde{X}\,^2\Pi$ and $\tilde{a}\,^4\Sigma^-$ states. Both states are accessible from the $C_{2n}N^-\,^3\Sigma^-$ states, which have a [core] $\pi^4\sigma^2\pi^2$ molecular orbital (MO) configuration. Removal of an electron from the highest occupied π or σ MO produces the neutral $\tilde{X}\,^2\Pi$ or $\tilde{a}\,^4\Sigma^-$ state, respectively. As shown previously,[35,40] photodetachment from π and σ MOs often proceeds via *s*+*d* and *p* scattering, respectively. We thus assign the lower energy band of peaks to the $\tilde{X}\,^2\Pi$ neutral ground state and the second band to the $\tilde{a}\,^4\Sigma^-$ first excited state, with both bands originating from the anion $^3\Sigma^-$ state. This assignment also implies that the $^3\Sigma^-$ state is the anion ground state rather than the bent singlet state found in the calculations of Zhan and Iwata,[32] since the $\tilde{a}\,^4\Sigma^-$ neutral state cannot be accessed by one-electron detachment from a singlet state of the anion. This point is considered in more detail below.

TABLE II. Peak positions, angular distributions, and assignments for the C_4N^- SEVI spectra.

Peak	Position (cm^{-1})	Offset (cm^{-1})	PAD	Assignments	
				Vibs	Electronic states
a	24 857	−237		6_1^1	$X\,^2\Pi \leftarrow X\,^3\Sigma^-$
b	25 013	−81		6_1^1	$X\,^2\Pi \leftarrow X\,^3\Sigma^-$
c	25 056	−38		6_1^1	$X\,^2\Pi \leftarrow X\,^3\Sigma^-$
A	25 094	0	*s*+*d*	0_0^0	$X\,^2\Pi_{1/2} \leftarrow X\,^3\Sigma^-$
B	25 123	29	*s*+*d*	0_0^0	$X\,^2\Pi_{3/2} \leftarrow X\,^3\Sigma^-$
C	25 377	283	*s*+*d*	6_0^2	$X\,^2\Pi \leftarrow X\,^3\Sigma^-$
D	27 271	2177	*s*+*d*	1_0^1	$X\,^2\Pi \leftarrow X\,^3\Sigma^-$
E	34 350	9256	*p*	0_0^0	$\tilde{a}\,^4\Sigma^- \leftarrow X\,^3\Sigma^-$
F	35 051	9957	*p*	4_0^1	$\tilde{a}\,^4\Sigma^- \leftarrow X\,^3\Sigma^-$

TABLE III. Peak positions, angular distributions, and assignments for the C_6N^- SEVI spectra.

Peak	Position (cm^{-1})	Offset (cm^{-1})	PAD	Assignments	
				Vibs	Electronic states
a	27 096	−97		9_1^1	$X\,^2\Pi \leftarrow X\,^3\Sigma^-$
b	27 142	−51		9_1^1	$X\,^2\Pi \leftarrow X\,^3\Sigma^-$
A	27 193	0	*s*+*d*	0_0^0	$X\,^2\Pi_{1/2} \leftarrow X\,^3\Sigma^-$
B	27 223	30	*s*+*d*	0_0^0	$X\,^2\Pi_{3/2} \leftarrow X\,^3\Sigma^-$
C	27 484	291	*s*+*d*	9_0^2	$X\,^2\Pi \leftarrow X\,^3\Sigma^-$
D	29 067	1874	*s*+*d*	3_0^1	$X\,^2\Pi \leftarrow X\,^3\Sigma^-$

For each species, the two main peaks of the $\tilde{X}\,^2\Pi$ bands, *A* and *B*, are assigned as transitions to the $\Pi_{1/2}$ and $\Pi_{3/2}$ spin-orbit components, respectively, of the vibrational ground state. In C_2N, the splitting between those two peaks is 38 cm^{-1}, which is in good agreement with the 40.3799 cm^{-1} effective spin-orbit splitting derived from rotationally resolved absorption spectroscopy.[11] In C_4N and C_6N, these peaks are spaced by 29 and 30 cm^{-1}, respectively, and represent the first experimental determination of the spin-orbit splitting in these species. These spin-orbit splittings are noticeably smaller than the value of 40 cm^{-1} assumed by McCarthy *et al.*[25] in fitting their C_4N and C_6N microwave spectra to a model Hamiltonian; no transitions involving the $\Pi_{3/2}$ component were observed in their study.

From the eBE of the peaks labeled *A*, we obtain the first experimental electron affinities (EAs) of C_2N, C_4N, and C_6N. These values are $EA(C_2N)=2.7489\pm0.0010$ eV, $EA(C_4N)=3.1113\pm0.0010$ eV, and $EA(C_6N)=3.3715\pm0.0010$ eV. The calculated EAs, including zero-point energy corrections, are 2.92, 3.29, and 3.56 eV for C_2N, C_4N, and C_6N, respectively. The B3LYP calculations overestimate the EA of these species by around 0.2 eV. Our experimental electron affinities and spin-orbit splittings are listed in Table V.

In the $\tilde{X}\,^2\Pi$ bands, the small peaks *C* are too close to the band origin to be any of the stretching modes, according to our calculations, and hence must be from transitions to bend-

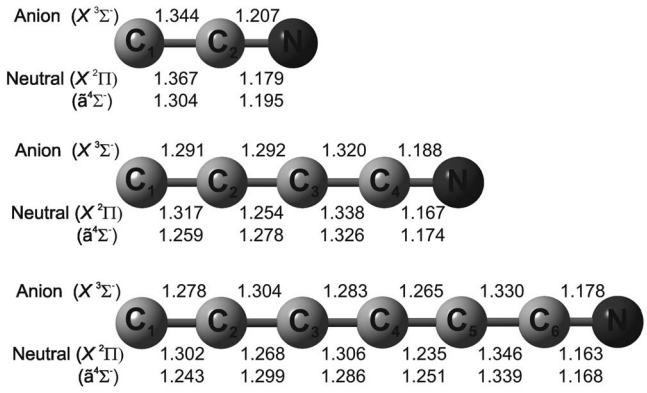

FIG. 5. Anion and neutral geometries calculated at the B3LYP/aug-cc-pVTZ level.

TABLE IV. Calculated relative energies and harmonic vibrational frequencies (cm^{-1}) at the B3LYP/aug-cc-pVTZ level of theory.

	State	ΔE (eV)	ν_1	ν_2	ν_3	ν_4	ν_5	ν_6	ν_7	ν_8	ν_9	ν_{10}	ν_{11}
C_2N			σ	π_x/π_y	σ								
Anion	$X\ ^3\Sigma^-$	−2.92	1749	465	1116								
Neutral	$X\ ^2\Pi$	0.00	2216	261/400	1078								
	$\tilde{a}\ ^4\Sigma^-$	1.10	1772	463	1240								
C_4N			σ	σ	σ	σ	π_x/π_y	π_x/π_y	π_x/π_y				
Anion	$X\ ^3\Sigma^-$	−3.29	2009	1830	1473	752	481	394	119				
Neutral	$X\ ^2\Pi$	0.00	2179	1986	1419	752	442/585	355/302	114/132				
	$\tilde{a}\ ^4\Sigma^-$	1.16	2070	1749	1559	765	457	404	128				
C_6N			σ	σ	σ	σ	σ	σ	π_x/π_y	π_x/π_y	π_x/π_y	π_x/π_y	π_x/π_y
Anion	$X\ ^3\Sigma^-$	−3.56	2113	1973	1847	1613	1067	559	495	483	385	186	77
Neutral	$X\ ^2\Pi$	0.00	2242	2091	1953	1558	1068	559	538/612	446/481	321/366	181/182	77/79
	$\tilde{a}\ ^4\Sigma^-$	1.17	2165	2011	1681	1665	1083	562	502	452	392	197	79

excited neutral levels. In order to assign these peaks, we have to consider the RT coupling that affects the bending modes in the $\tilde{X}\ ^2\Pi$ states of the $C_{2n}N$ radicals. In C_2N, the vibronic bending levels for $v_2 \leq 2$ obtained using the RT parameters determined by Kohguchi *et al.*[19] are presented in Fig. 6. In the absence of additional vibronic coupling, the lowest vibrational bending level accessible by photodetachment from the C_2N^- anion ground state is the $(020)\mu\Pi_r$ doublet. These levels have never been directly observed experimentally but are calculated to lie 454.4 and 458.9 cm^{-1} above the origin transition. Peak *C* in C_2N, which lies 456 cm^{-1} from peak *A*, is thus assigned to the $2_0^{2(\mu\Pi)}$ transition with the individual doublet components being too close to be resolved in our experiment.

By analogy, peak *C* in each of the C_4N^- and C_6N^- spectra is also likely to involve excitation of neutral bending levels. In C_4N, this feature is shifted by 283 cm^{-1} from peak *A* and can be either the $6_0^{2(\mu\Pi)}$ or $7_0^{2(\mu\Pi)}$ transition based on the B3LYP frequencies in Table IV. Similarly, in C_6N, peak *C* is spaced 291 cm^{-1} from peak *A* and could be either the $9_0^{2(\mu\Pi)}$ or the $10_0^{2(\mu\Pi)}$ transition. Based on the calculated frequencies alone, it might seem more reasonable to assign peak *C* to $7_0^{2(\mu\Pi)}$ in C_4N and $10_0^{2(\mu\Pi)}$ in C_6N. However, the anion and neutral harmonic frequencies for these modes are very similar; this situation generally results in extremely weak $\Delta v \neq 0$ transitions for a nontotally symmetric vibrational mode. Larger calculated changes in frequency are found for the v_6 and v_9 modes in C_4N and C_6N, respectively, and the artifactual splitting of the degeneracy is considerably higher, which is generally a signature of stronger RT coupling. This coupling, in turn, can significantly lower the energy of the $6_0^{2(\mu\Pi)}$ and $9_0^{2(\mu\Pi)}$ transitions, in analogy to the situation in C_2N, so assignment of peak *C* to these transitions may be preferable. More definitive assignments require a fuller understanding of RT coupling in C_4N and C_6N.

In the $\tilde{X}\ ^2\Pi$ band of C_4N^- and C_6N^-, there is also a small peak labeled *D*. In C_4N, this peak is located 2177 cm^{-1} from the origin and is assigned to the 1_0^1 transition, based on our calculation of 2179 cm^{-1} for the fundamental of the v_1 mode, the C_3C_4N asymmetric stretch. In C_6N, peak *D* is shifted 1874 cm^{-1} from the origin. This shift is close to our calculated frequency of 1953 cm^{-1} for the v_3 mode, primarily a $C_2C_3C_4$ asymmetric stretching motion, so peak *D* in this case is assigned to the 3_0^1 transition. The

TABLE V. Experimental electron affinity, ground state spin-orbit splitting, and $\tilde{a}\ ^4\Sigma^-$ state term energy of C_2N, C_4N, and C_6N.

	EA (eV) (±0.0010)	S–O splitting ($X\ ^2\Pi$) (cm^{-1})	T_0 ($\tilde{a}\ ^4\Sigma^-$) (eV) (±0.0010)
C_2N	2.7489	38 (40.3799)[a]	1.0431
C_4N	3.1113	29	1.1476
C_6N	3.3715	30	⋯

[a]From Ref. 11.

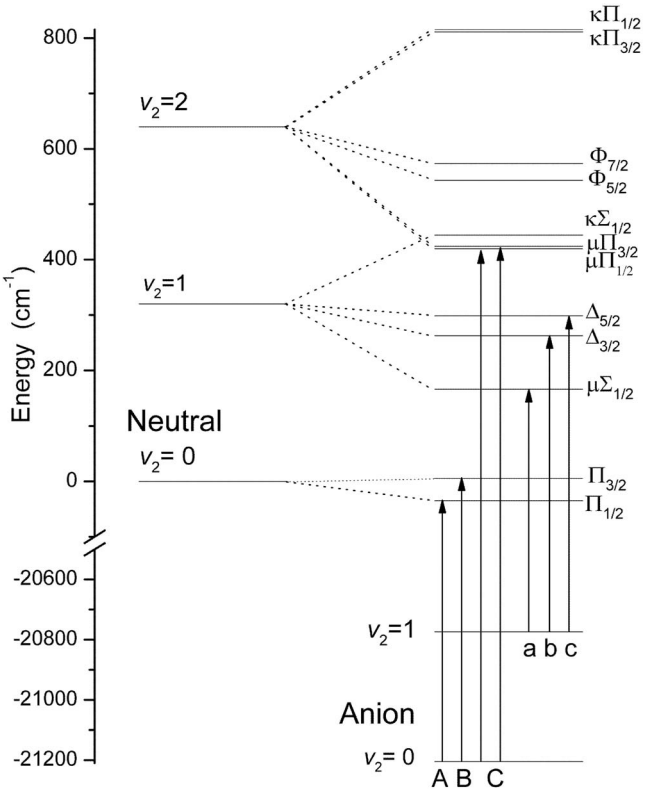

FIG. 6. The C_2N ($X\ ^2\Pi$) vibronic bending levels for $v_2 \leq 2$ (from Ref. 19) and the observed transitions in the SEVI spectra.

assignment of these peaks is also in agreement with Franck–Condon simulations (not shown) which show that υ_1 and υ_3 are the only stretching modes with significant activity in the $\tilde{X}\,^2\Pi$ bands of C_4N and C_6N, respectively.

In the $\tilde{X}\,^2\Pi$ bands, there are as many as three small peaks labeled *a*, *b*, and *c* below the vibrational origin. These peaks are assigned to transitions originating from excited vibrational states in the anion. Because the main spectral feature is the 0_0^0 transition, one expects the small peaks to be sequence bands with $\Delta\upsilon=0$. The most likely populated vibrational levels in the anions are the low-frequency bending modes. In C_2N, the (010) mode of the neutral is split into four levels by RT coupling (see Fig. 6); all four are accessible by photodetachment from the anion (010) level. In Fig. 2(a), peaks *a* and *b* are split by 95 cm^{-1}, close to the calculated splitting of 96.6 cm^{-1} between the $(010)\mu\Sigma$ and $(010)\Delta_{3/2}$ levels. Similarly, peaks b and c are split by 37 cm^{-1} which is very close to the calculated splitting of 36.2 cm^{-1} between the $(010)\Delta_{3/2}$ and $(010)\Delta_{5/2}$ levels. Peaks a, b and c in the C_2N spectra are thus assigned to the $2_1^{1(\mu\Sigma)}$, $2_1^{1(\Delta_{5/2})}$, and $2_1^{1(\Delta_{3/2})}$ transitions respectively. The $2_1^{1(\kappa\Sigma)}$ transition is probably also present but is calculated to be buried under peak *B*. Using the experimentally known energy of the $(010)\mu\Sigma$ level,[19] this assignment implies that the υ_2 fundamental of the C_2N^- anion is 432 cm^{-1}. This value is in reasonable agreement with the calculated frequency of 465 cm^{-1} in Table IV, thereby supporting the proposed assignments.

Again, RT coupling analysis in C_4N and C_6N is required to fully assign the sequence bands in the spectra of these species. The pattern of these peaks in C_4N spectrum is very similar to that in C_2N, suggesting a similar assignment. These peaks are probably the 6_1^1 transitions in C_4N because our calculations suggest a large RT splitting for this mode as well as a significant change in anion versus neutral frequency, both of which are necessary to see multiple, distinct sequence bands. For similar reasons, the sequence bands in the C_6N spectrum are most likely 9_1^1 transitions.

The lower panels of Figs. 2(b) and 3(b) display features assigned to the $\tilde{a}\,^4\Sigma^-$ excited electronic states of C_2N and C_4N, respectively. These spectra represent the first experimental observation of the quartet states. The dominant peak of each quartet band, labeled E, is assigned to the 0_0^0 transition. The term energy of the C_2N $\tilde{a}\,^4\Sigma^-$ state is thus determined to be 1.0431 ± 0.0010 eV. This value agrees with our calculation which predicted a term energy of 1.10 eV for this state. The 1.03 eV value calculated by Pd and Chandra[24] at the higher CASSCF level is also in excellent agreement with experiment. The term energy of the C_4N $\tilde{a}\,^4\Sigma^-$ state is determined to be 1.1476 ± 0.0010 eV, in excellent agreement with the value of 1.16 eV calculated at the B3LYP level. Note that our calculations indicate that C_6N also has a quartet state lying 1.17 eV above the ground state. However, the detachment photon energy required to access this state is higher than the maximum available with our current laser setup and it could not be observed. The experimental quartet term energies obtained here are listed in Table V.

In the C_2N $\tilde{a}\,^4\Sigma^-$ band, the smaller peak, labeled *F*, is assigned to the 3_0^1 transition. This yields a frequency of the υ_3 fundamental of 1170 cm^{-1}, which is slightly smaller than the value of 1240 cm^{-1} calculated in this work and larger than the 1101 cm^{-1} value calculated at the CASSCF level by Pd and Chandra.[24] Similarly, the peak labeled *E* in the C_4N $\tilde{a}\,^4\Sigma^-$ band is assigned to the 4_0^1 transition. The υ_4 mode is a symmetric stretch of the carbon chain. This assignment yields a frequency of 701 cm^{-1} for the υ_4 fundamental which is close to our calculated value of 765 cm^{-1}.

The SEVI spectra presented here address a key issue regarding the electronic structure and geometry of the anion ground states. The $C_{2n}N^-$ anions have close-lying singlet and triplet states with calculated relative energies that depend on the method used.[32,33] Zhan and Iwata[32] used the MP2 method to investigate the structure of the C_nN^- $(n=1-13)$ anions. They found a singlet ground state for all the $C_{2n}N^-$ species with the $n>1$ chains having strongly bent structures. For C_4N^- and C_6N^-, linear triplet states were found to be 0.368 and 0.822 eV above the singlet ground state, respectively. A subsequent study by Pascoli and Lavendy[33] using DFT/B3LYP predicted a linear triplet ground state $(^3\Sigma^-)$ for the $C_{2n}N^-$ $(n=1-3)$ anions. A coupled-cluster, single-point energy calculation on the B3LYP optimized geometries located the bent singlet excited state $(^1A')$ of C_2N^-, C_4N^-, and C_6N^- with term energies of 0.75, 0.25, and 0.22 eV, respectively. The discrepancy between the two methods was attributed to high spin contamination of the Hartree–Fock reference wave function for the linear triplet state in the MP2 calculations.[33]

All SEVI spectra reported here are dominated by the origin (0_0^0) transition and display a small number of transitions to excited vibrational levels. This pattern is consistent with the anion and neutral states having similar geometries. Since it is known from microwave spectroscopy experiments[21,25] that C_2N, C_4N, and C_6N all have linear ground states, the anions must also be linear in accordance with the DFT calculations.[33] If the C_4N^- and C_6N^- anions had strongly bent geometries, such as those predicted by MP2 calculations, extended progressions of bending modes would be seen. Moreover, the quartet states of C_2N and C_4N are not accessible by one-electron detachment from an anion singlet state. We thus conclude that the $C_{2n}N^-$ $(n=1-3)$ anions have linear $^3\Sigma^-$ ground states and that the singlet excited state is too high in energy to be significantly populated.

VI. CONCLUSIONS

High resolution photoelectron spectra of C_2N^-, C_4N^-, and C_6N^- obtained using SEVI are reported. This work provides the first measurement of the adiabatic electron affinities of the three species as well as the term energy of the low-lying $\tilde{a}\,^4\Sigma^-$ state of C_2N and C_4N. The spin-orbit splitting in the $\tilde{X}\,^2\Pi$ ground state of C_4N and C_6N is also experimentally determined for the first time. The observation of relatively little vibrational activity and transitions to neutral quartet states in the photoelectron spectra indicates that the $C_{2n}N^-$ $(n=1-3)$ anions all have linear $^3\Sigma^-$ ground states, in agreement with the theoretical study of Pascoli and Lavendy.[33]

ACKNOWLEDGMENTS

This work was supported by the Air Force Office of Scientific Research under Grant No. F49620-03-1-0085. E.G. thanks the National Science and Engineering Research Council of Canada (NSERC) for a post graduate scholarship and T.I.Y. thanks the Fonds Québécois de la Recherche sur la Nature et les Technologies (FQRNT) for a master's scholarship.

[1] A. McKellar, Publ. Astron. Soc. Pac. **52**, 307 (1940).
[2] M. Guelin and P. Thaddeus, Astrophys. J. **212**, L81 (1977).
[3] P. Friberg, A. Hjalmarson, W. M. Irvine, and M. Guelin, Astrophys. J. **241**, L99 (1980).
[4] M. Guelin, N. Neininger, and J. Cernicharo, Astron. Astrophys. **335**, L1 (1998).
[5] P. Thaddeus, C. A. Gottlieb, H. Gupta, S. Brunken, M. C. McCarthy, M. Agundez, M. Guelin, and J. Cernicharo, Astrophys. J. **677**, 1132 (2008).
[6] T. I. Hasegawa and E. Herbst, Mon. Not. R. Astron. Soc. **263**, 589 (1993).
[7] S. D. Doty and C. M. Leung, Astrophys. J. **502**, 898 (1998).
[8] F. Pauzat, Y. Ellinger, and A. D. McLean, Astrophys. J. **369**, L13 (1991).
[9] A. J. Merer and D. N. Travis, Can. J. Phys. **43**, 1795 (1965).
[10] V. E. Bondybey and J. H. English, J. Mol. Spectrosc. **70**, 236 (1978).
[11] M. Kakimoto and T. Kasuya, J. Mol. Spectrosc. **94**, 380 (1982).
[12] K. Kawaguchi, T. Suzuki, S. Saito, E. Hirota, and T. Kasuya, J. Mol. Spectrosc. **106**, 320 (1984).
[13] M. Feher, C. Salud, J. P. Maier, and A. J. Merer, J. Mol. Spectrosc. **150**, 280 (1991).
[14] M. Feher, C. Salud, and J. P. Maier, J. Mol. Spectrosc. **145**, 246 (1991).
[15] S. A. Beaton, D. A. Gillett, J. M. Brown, M. Feher, and A. Rohrbacher, J. Mol. Spectrosc. **209**, 60 (2001).
[16] K. Hakuta and H. Uehara, J. Chem. Phys. **78**, 6484 (1983).
[17] K. Hakuta, H. Uehara, K. Kawaguchi, T. Suzuki, and T. Kasuya, J. Chem. Phys. **79**, 1094 (1983).
[18] C. R. Brazier, L. C. Obrien, and P. F. Bernath, J. Chem. Phys. **86**, 3078 (1987).
[19] H. Kohguchi, Y. Ohshima, and Y. Endo, J. Chem. Phys. **106**, 5429 (1997).
[20] N. Oliphant, A. Lee, P. F. Bernath, and C. R. Brazier, J. Chem. Phys. **92**, 2244 (1990).
[21] Y. Ohshima and Y. Endo, J. Mol. Spectrosc. **172**, 225 (1995).
[22] M. D. Allen, K. M. Evenson, D. A. Gillett, and J. M. Brown, J. Mol. Spectrosc. **201**, 18 (2000).
[23] W. Gabriel, E. A. Reinsch, and P. Rosmus, Chem. Phys. Lett. **231**, 13 (1994).
[24] R. Pd and P. Chandra, J. Chem. Phys. **114**, 1589 (2001).
[25] M. C. McCarthy, G. W. Fuchs, J. Kucera, G. Winnewisser, and P. Thaddeus, J. Chem. Phys. **118**, 3549 (2003).
[26] J. J. Belbruno, Z. C. Tang, R. Smith, and S. Hobday, Mol. Phys. **99**, 957 (2001).
[27] Y. H. Ding, J. L. Liu, X. R. Huang, Z. S. Li, and C. C. Sun, J. Chem. Phys. **114**, 5170 (2001).
[28] K. Chuchev and J. J. Belbruno, J. Phys. Chem. A **106**, 4240 (2002).
[29] R. B. Huang, C. R. Wang, Z. Y. Liu, L. S. Zheng, F. Qi, L. S. Sheng, S. Q. Yu, and Y. W. Zhang, Z. Phys D: At. Mol. Clusters **33**, 49 (1995).
[30] C. R. Wang, R. B. Huang, Z. Y. Liu, and L. S. Zheng, Chem. Phys. Lett. **237**, 463 (1995).
[31] A. K. Gupta and P. Ayyub, Eur. Phys. J. D **17**, 221 (2001).
[32] C. G. Zhan and S. Iwata, J. Chem. Phys. **104**, 9058 (1996).
[33] G. Pascoli and H. Lavendy, Chem. Phys. Lett. **312**, 333 (1999).
[34] A. Osterwalder, M. J. Nee, J. Zhou, and D. M. Neumark, J. Chem. Phys. **121**, 6317 (2004).
[35] J. Zhou, E. Garand, and D. M. Neumark, J. Chem. Phys. **127**, 114313 (2007).
[36] D. M. Neumark, J. Phys. Chem. A **112**, 13287 (2008).
[37] A. Eppink and D. H. Parker, Rev. Sci. Instrum. **68**, 3477 (1997).
[38] U. Even, J. Jortner, D. Noy, N. Lavie, and C. Cossart-Magos, J. Chem. Phys. **112**, 8068 (2000).
[39] D. L. Osborn, D. J. Leahy, D. R. Cyr, and D. M. Neumark, J. Chem. Phys. **104**, 5026 (1996).
[40] J. Zhou, E. Garand, W. Eisfeld, and D. M. Neumark, J. Chem. Phys. **127**, 034304 (2007).
[41] J. Zhou, E. Garand, and D. M. Neumark, J. Chem. Phys. **127**, 154320 (2007).
[42] W. C. Wiley and I. H. McLaren, Rev. Sci. Instrum. **26**, 1150 (1955).
[43] D. W. Chandler and P. L. Houston, J. Chem. Phys. **87**, 1445 (1987).
[44] E. W. Hansen and P. L. Law, J. Opt. Soc. Am. A **2**, 510 (1985).
[45] J. Cooper and R. N. Zare, J. Chem. Phys. **48**, 942 (1968).
[46] K. L. Reid, Annu. Rev. Phys. Chem. **54**, 397 (2003).
[47] M. J. Nee, A. Osterwalder, J. Zhou, and D. M. Neumark, J. Chem. Phys. **125**, 014306 (2006).
[48] K. Chuchev and J. J. Belbruno, J. Phys. Chem. A **107**, 1887 (2003).
[49] A. D. Becke, J. Chem. Phys. **98**, 1372 (1993).
[50] C. T. Lee, W. T. Yang, and R. G. Parr, Phys. Rev. B **37**, 785 (1988).
[51] T. H. Dunning, J. Chem. Phys. **90**, 1007 (1989).
[52] M. J. Frisch, G. W. Trucks, H. B. Schlegel *et al.*, GAUSSIAN 03, Revision C.02, Gaussian, Inc., Wallingford, CT, 2004.